Statistics of nodal points of in-plane random waves in elastic media

Dmitrii N. Maksimov and Almas F. Sadreev
Institute of Physics, Academy of Sciences, 660036 Krasnoyarsk, Russia
(Received 31 December 2007; published 8 May 2008)

We consider the nodal points (NPs) $u=0$ and $v=0$ of the in-plane vectorial displacements $\mathbf{u}=(u,v)$ which obey the Navier-Cauchy equation. Similar to the Berry conjecture of quantum chaos, we present the in-plane eigenstates of chaotic billiards as the real part of the superposition of longitudinal and transverse plane waves with random phases. By an average over random phases we derive the mean density and correlation function of NPs. Consequently we consider the distribution of the nearest distances between NPs.

DOI: 10.1103/PhysRevE.77.056204 PACS number(s): 05.45.Ac, 62.30.+d, 46.40.Cd, 46.40.−f

I. INTRODUCTION

Attracting interest in the field of wave chaos, elastomechanical systems are being studied analytically, numerically, and experimentally. Weaver first measured the few hundred lower eigenfrequencies of an aluminum block and worked out the spectral statistics [1]. Spectral statistics coinciding with random matrix theory has been observed in experiments for monocrystalline quartz blocks shaped as three-dimensional Sinai billiards [2], as well as in experimental and numerical studies of flexural modes [3,4] and in-plane modes [5,6] for stadium-shaped plates. Statistical properties of eigenfunctions describing standing waves in elastic billiards were first reported by Schaadt *et al.* [7]. The authors measured the displacement field of several eigenmodes of a thin plate shaped as a Sinai stadium.

Due to a good preservation of up-down symmetry in the case of thin plates, they dealt with two types of modes. The flexural modes with displacement ψ perpendicular to the plane of the plate are well described by the scalar biharmonic Kirchoff-Love equation [8,9]

$$D\nabla^4\psi = \rho h\Omega^2\psi. \tag{1}$$

Here, h is the thickness of the plate and D denotes the flexural rigidity, given by $D=Eh^3/12(1-\sigma^2)$, where E is Young's modulus, σ is Poisson's ratio, and ρ is the density. Solutions of Eq. (1) are characterized by nodal lines near which fine powder is collected under vibrations which are visualized as Chladni patterns [10]. As it is dependent on the size of fine particles, a very thin powder can collect at antinodal regions where the amplitude of vibrations is maximal [11–13].

Other modes have vectorial displacement in the plane of the plate. They are described by a two-dimensional Navier-Cauchy equation for the in-plane displacement vector [9,14]:

$$\mu\nabla^2\mathbf{u} + (\lambda+\mu)\,\boldsymbol{\nabla}\,(\boldsymbol{\nabla}\cdot\mathbf{u}) + \rho\Omega^2\mathbf{u} = 0, \tag{2}$$

where $\mathbf{u}(x,y)$ is the displacement field in the plate and λ and μ are the material-dependent Lamé coefficients. Introducing the elastic potentials ψ and $\mathbf{A}$ with the help of the Helmholtz [14] decomposition the displacement field $\mathbf{u}$ can be written as

$$\mathbf{u} = \mathbf{u}_l + \mathbf{u}_t, \quad \mathbf{u}_l = \boldsymbol{\nabla}\psi, \quad \mathbf{u}_t = \boldsymbol{\nabla}\times\mathbf{A}. \tag{3}$$

Then Eq. (2) reduces to two Helmholtz equations for the elastic potentials:

$$-\nabla^2\psi = k_l^2\psi,$$

$$-\nabla^2\mathbf{A} = k_t^2\mathbf{A}. \tag{4}$$

Here $k_l=\omega/c_l$ and $k_t=\omega/c_t$ are the wave numbers for the longitudinal and transverse waves, respectively, and $\omega^2=\rho\Omega^2/E$. In the two-dimensional case the potential $\mathbf{A}$ has only one nonzero component A_z, and the dimensionless longitudinal and transverse sound velocities $c_{l,t}$ are given by

$$c_l^2 = \frac{1}{1-\sigma^2}, \quad c_t^2 = \frac{1}{2(1+\sigma)}, \tag{5}$$

where σ is Poisson's ratio [9,14]. σ is a function of the Lamé coefficients [9,14].

In chaotic elastic billiards the in-plane eigenstates can be simulated by the real part of the random superposition of longitudinal and transverse plane waves [15]:

$$u(\mathbf{x}) = \sqrt{\frac{2(1-\gamma)}{N}}\sum_{n=1}^{N}\cos\,\phi_{ln}\cos[i(\mathbf{k}_{ln}\cdot\mathbf{x}+\theta_{ln})] + \sqrt{\frac{2\gamma}{N}}\sum_{n=1}^{N}\sin\,\phi_{tn}\cos[i(\mathbf{k}_{tn}\cdot\mathbf{x}+\theta_{tn})],$$

$$v(\mathbf{x}) = \sqrt{\frac{2(1-\gamma)}{N}}\sum_{n=1}^{N}\sin\,\phi_{ln}\cos[i(\mathbf{k}_{ln}\cdot\mathbf{x}+\theta_{ln})] - \sqrt{\frac{2\gamma}{N}}\sum_{n=1}^{N}\cos\,\phi_{tn}\cos[i(\mathbf{k}_{tn}\cdot\mathbf{x}+\theta_{tn})], \tag{6}$$

where ϕ_{ln} and ϕ_{tn} are the angles between $\mathbf{k}_{ln}$ and $\mathbf{k}_{tn}$ and the x axis, respectively. The prefactors $\sqrt{\gamma}$ and $\sqrt{1-\gamma}$ are chosen from the normalization condition $\langle\mathbf{u}^\dagger\mathbf{u}\rangle=1$, and $\langle\cdots\rangle$ means an average over the random phase ensembles. This superposition originates from Berry's conjecture for quantum chaos [16–22] for each solution of the Helmholtz equations (4). The parameter γ ranges from 0 (pure transverse waves) to 1 (pure longitudinal waves) for an infinite system and takes a specific value

$$\gamma = \frac{c_t^2}{c_t^2 + c_l^2} \tag{7}$$

for closed billiards [15] because of double ray splitting at its boundary.

Here we derive the nodal-point (NP) density correlation function of the vectorial in-plane elastic field (6) and statistics of the nearest distances between NPs considered in [23–30] for quantum chaos. Similar to the Chladni patterns at nodal lines for the flexural modes [10,12], one can be interested in the NPs of in-plane modes as centers of the collection of viscous powder. For closed elastic plate (billiard) the vectorial in-plane displacements $\mathbf{u}(x,y) = u(x,y)v(x,y)$ have NPs

$$u(x_0,y_0) = 0, \quad v(x_0,y_0) = 0, \tag{8}$$

at the point $\mathbf{x}_0 = (x_0, y_0)$. NPs of vectorial field are specified by the Poincaré index (topological charge) [31]. Here, we consider the statistical properties of NPs in elastic random waves. In this case, only structurally stable zeros of the Poincaré indices $q \pm 1$ occur [29]:

$$q = \mathrm{sgn}(\det M_{\mathbf{x}_0}) = \mathrm{sgn}(\lambda_1\lambda_2), \quad M = \begin{pmatrix} \frac{\partial u}{\partial x} & \frac{\partial u}{\partial y} \\ \frac{\partial v}{\partial x} & \frac{\partial v}{\partial y} \end{pmatrix}, \tag{9}$$

where $\lambda_{1,2}$ are eigenvalues of matrix M at NP $\mathbf{x}_0$. Depending on these eigenvalues NPs split on the four types [31]: (i) centers for imaginary $\lambda_{1,2}$ with the index $q=1$, (ii) nodes for real $\lambda_{1,2}$ with the same sign and $q=1$, (iii) focuses for complex $\lambda_1 = \lambda_2^*$ with $q=1$, and (iv) saddles for real $\lambda_{1,2}$ with opposite sign and $q=-1$. Eigenvalues of the matrix M are $\frac{u_x+v_y}{2} \pm \sqrt{(\frac{u_x+v_y}{2})^2 - J} = \frac{u_x+v_y}{2} \pm \sqrt{D}/4$ where we have introduced

$$S = (u_x + v_y)^2 - 4J, \quad J = \det(M). \tag{10}$$

If $q=1$ and $S>0$, the NP can be classified as node, while for $q=1$ and $S<0$ we have the NP as focus (center for the particular case $u_x+v_y=0$). At last for $q=-1$ the NP is a saddle.

In order to clearly show these types of NPs we consider the simple superposition (6) consisting of only three plane waves with the wave vectors directed by $2\pi/3$ angles relative to each other. Moreover, we exclude all random phases in the exponents. For $\gamma=1$ we have the vectorial "electric" field $\mathbf{u}=\nabla\psi$. Then at the NP the "scalar potential" ψ achieves maximum or minimum for $q=1$ or has a saddle point for $q=-2$. Respectively, the NP of $\mathbf{u}$ is a node or a saddle as demonstrated in Fig. 1. For $\gamma=1$ we have the vectorial "magnetic" field $\mathbf{u}=\nabla\times\mathbf{A}$ the NPs of which are centers of displacements and saddles as demonstrated in Fig. 2.

II. MEAN DENSITY OF NPs

A fragment of the vectorial in-plane random displacement (u,v), Eq. (6), shown in Fig. 3 illustrates the nodal lines of u and v and NPs at the intersection of them. Each NP can be specified by the winding number $q=\pm 1$ which is exactly the Poincaré index (9) [32,33] marked in Fig. 3 by circles and crosses, respectively. There is a close relation between nodal points with opposite q as discussed in [34,35]. As one can see from Fig. 3 at each nodal line the nearest NPs have the opposite Poincaré index.

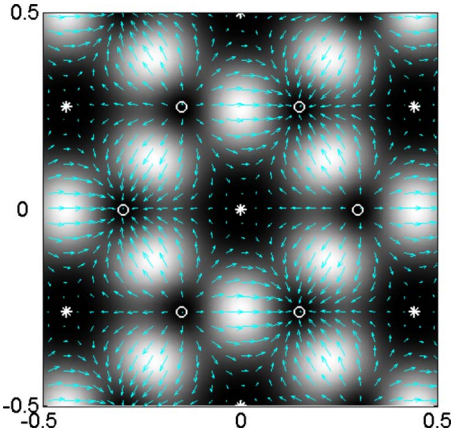

FIG. 1. (Color online) Intensity of in-plane displacement u^2+v^2 and vectorial field $\mathbf{u}=\nabla\psi$ shown by arrows for the superposition of three plane longitudinal waves with the wave vectors directed by $2\pi/3$ angles relative each other and zero random phases $\theta_{ln}=0$. $k_l=20$ and $\sigma=0.5$. NPs are shown by circles (nodes) and by stars (saddles).

It is known that the density of NPs for a two-dimensional complex random Gaussian field (RGF) $[\psi(x,y)=u(x,y)+iv(x,y)]$ equals $k^2/4\pi$ [25,26]. Consider the density of NPs for the case of an elastic vectorial field also given by the RGF (6). We have for the NP density

$$\rho = \langle \delta(u)\delta(v)|J|\rangle, \tag{11}$$

where the Jacobian M is given by formula (9). We eliminate the modulus sign in (11) using the identity

$$\mathrm{sgn}(x) = \frac{1}{i\pi}\int_{-\infty}^{\infty} \frac{e^{i\omega x}}{\omega} d\omega, \tag{12}$$

to rewrite (11) as

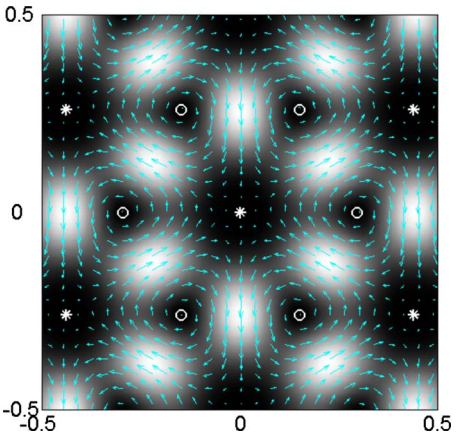

FIG. 2. (Color online) Intensity of in-plane displacement u^2+v^2 and vectorial field $\mathbf{u}=\nabla\times\mathbf{A}$ for the superposition of three plane transverse waves with the wave vectors directed by $2\pi/3$ angles relative each other and zero random phases $\theta_{tn}=0$. $k=10$ and $\sigma=0.5$. Saddles are shown by stars and centers by circles.

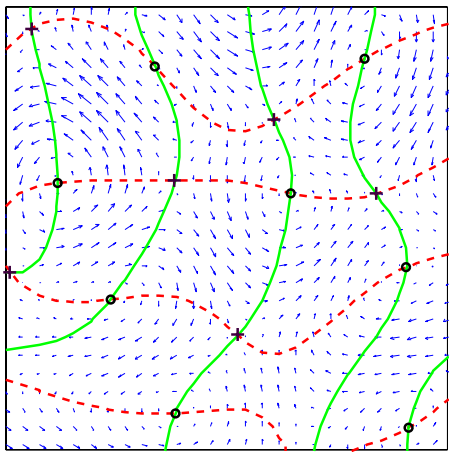

FIG. 3. (Color online) Random superposition of 100 waves for $\sigma=0.345$. γ is given by (7). The nodal lines of components u and v are shown by solid and dashed lines. Their intersections result in focuses with the Poincaré index +1 (circles) and saddles with the Poincaré index −1 (crosses).

$$\rho = -\frac{1}{\pi}\int_{-\infty}^{\infty}\frac{1}{\omega}\frac{\partial\langle\delta(u)\delta(v)e^{i\omega J}\rangle}{\partial\omega}d\omega. \tag{13}$$

An average $\langle\cdots\rangle$ implies here integration over two RGFs u and v and their four derivatives u_x, u_y, v_x, and v_y. Introducing the total sixfold Gaussian random vector $\Psi=(u,u_x,u_y,v,v_x,v_y)$ we write the average as integration over Ψ [20]:

$$\langle\delta(u)\delta(v)\exp(i\omega J)\rangle = \frac{1}{(2\pi)^3\sqrt{\det\hat{\Sigma}_1}}\int\delta(u)\delta(v) \times\exp(i\omega J - \Psi\hat{\Sigma}_1^{-1}\Psi^T/2)d^6\Psi, \tag{14}$$

where T marks the transposed vector Ψ and the 6×6 correlation matrix is $\hat{\Sigma}_1=\langle\Psi^T\Psi\rangle$. Straightforward easy integration over random phases of random Gaussian wave (6) gives the correlation matrix as

$$\hat{\Sigma}_1 = \begin{pmatrix} 1/2 & 0 & 0 & 0 & 0 & 0 \\ 0 & f & 0 & 0 & 0 & l \\ 0 & 0 & g & 0 & l & 0 \\ 0 & 0 & 0 & 1/2 & 0 & 0 \\ 0 & 0 & l & 0 & g & 0 \\ 0 & l & 0 & 0 & 0 & f \end{pmatrix}, \tag{15}$$

where (see the Appendix)

$$f = \frac{3}{8}\gamma k_l^2 + \frac{1}{8}(1-\gamma)k_t^2,$$

$$g = \frac{1}{8}\gamma k_l^2 + \frac{3}{8}(1-\gamma)k_t^2,$$

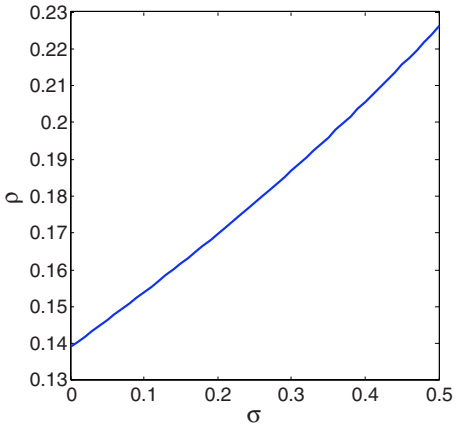

FIG. 4. (Color online) The NP density versus σ. $\omega=1$.

$$l = \frac{1}{8}\gamma k_l^2 - \frac{1}{8}(1-\gamma)k_t^2. \tag{16}$$

Note that for the in-plane random waves in elastic media the mean values $\langle u_x v_y\rangle$ and $\langle u_y v_x\rangle$ are not zero.

The matrix (15) decomposes into

$$\frac{1}{2}\oplus\frac{1}{2}\oplus\begin{pmatrix} f & l \\ l & f \end{pmatrix}\oplus\begin{pmatrix} g & l \\ l & g \end{pmatrix}.$$

Then the inverse matrix $\hat{K}^{-1}$ can be easily found. As a result, integration over the couples (u_x,v_y) and (u_y,v_x) in (14) gives the expression

$$\frac{1}{2\pi}\frac{1}{[(l+g)i\omega-1]}\frac{1}{\sqrt{[1+(f+l)i\omega][1+(g-l)i\omega]}}. \tag{17}$$

Here in accordance with (16) we used that $g+l=f-l$. Substituting (17) into (13) we obtain finally for the mean density of NPs

$$\rho = \frac{[\gamma k_l^2 + (1-\gamma)k_t^2]^2}{2\pi\sqrt{\gamma k_l^2 + 3(1-\gamma)k_t^2}\sqrt{3\gamma k_l^2 + (1-\gamma)k_t^2}}. \tag{18}$$

As seen from (6), this expression cannot be limited to the known mean density of NPs for the Berry function $k^2/4\pi$ even for $\gamma=0$ or $\gamma=1$. The parameter γ that superposes the longitudinal and transverse random waves is arbitrary. In elastic billiards it depends only on the material parameter, the Poisson ratio σ as given by (5) and (7). Substituting this dependence into (18) we can find how the mean density depends on σ as shown in Fig. 4.

Similarly, we can introduce the mean density of saddles

$$\rho_s = \frac{1}{2}\langle\delta(u)\delta(v)|J|[1+\mathrm{sgn}(-J)]\rangle, \tag{19}$$

where the last factor excludes in (19) all cases of positive Poincaré indices. It is obvious for the random waves that $\rho_s=\frac{\rho}{2}$.

Moreover, one can consider the mean density of nodes and focus on which can be distinguished by a sign of (10) at corresponding NPs. Respectively, we write for the mean density of nodes and focuses

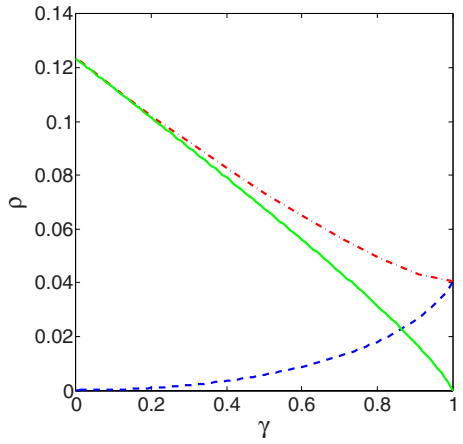

FIG. 5. (Color online) Dependence of the density of saddles (red dash-dotted line), focuses (green solid line), and nodes (blue dotted line) on γ for random in-plane waves given by (6). The material parameter $\sigma=0.345$ (aluminum). $\omega=1$.

$$\rho_{c,f} = \frac{1}{4}\langle \delta(u)\delta(v)|J|[1+\mathrm{sgn}(J)][1 \pm \mathrm{sgn}(S)]\rangle. \quad (20)$$

An evaluation of these integrals is rather cumbersome. More easy way is to perform the average numerically. The result is shown in Fig. 5.

III. CORRELATION FUNCTION OF NPs

The nodal density is defined by formula (11). The corresponding correlation function is [23–26]

$$G(s) = \frac{1}{\rho^2}\langle \delta(u)\delta(v)|J|\delta(u_s)\delta(v_s)|J_s|\rangle, \quad (21)$$

where for brevity we omitted the coordinate arguments of values except for the index s, which implies a distance between points $\mathbf{x}$ and $\mathbf{x}+s$. Similarly, the charge correlation function [23,25,26] gives the correlation of densities, but weighted with their Poincaré indices q:

$$G_q(s) = \frac{1}{\rho^2}\langle \delta(u)\delta(v)J\delta(u_s)\delta(v_s)J_s\rangle. \quad (22)$$

In the last formula there are no modules of Jacobians M and M_s. Therefore, a calculation of the charge correlation function (22) presents a simpler problem compared to the density correlation function $G(s)$.

An average $\langle\cdots\rangle$ implies integration over 12 RGFs $\varphi = (u, u_x, u_y, v, v_x, v_y, u^s, u^s_x, u^s_y, v^s, v^s_x, v^s_y)$ with 6 at point $\mathbf{x}$ and 6 at point $\mathbf{x}+s$:

$$\frac{1}{(2\pi)^6\sqrt{\det \hat{\Sigma}}}\int d^{12}\varphi\ \delta(u)\delta(v)\delta(u_s)\delta(v_s)JJ_s \times \exp\left(-\frac{1}{2}\varphi\hat{\Sigma}^{-1}\varphi^T\right), \quad (23)$$

with the 12×12 correlation matrix

$$\hat{\Sigma} = \langle \varphi^T\varphi\rangle = \begin{pmatrix} \hat{\Sigma}_1 & \hat{\Sigma}_2 \\ \hat{\Sigma}_2^T & \hat{\Sigma}_1 \end{pmatrix}, \quad (24)$$

where the matrix $\hat{\Sigma}_1$ is given by (15) while

$$\hat{\Sigma}_2 = \begin{pmatrix} A & C & 0 & 0 & 0 & D \\ -C & F & 0 & 0 & 0 & L \\ 0 & 0 & G & D & L & 0 \\ 0 & 0 & -D & B & E & 0 \\ 0 & 0 & L & -E & H & 0 \\ -D & L & 0 & 0 & 0 & I \end{pmatrix}. \quad (25)$$

Each matrix element depends on s, γ, and σ and can be evaluated by use of the random waves (6). The results are collected in the Appendix.

In order to calculate the integrals in (23) we use the approach developed by Dennis [29]. First, the 12×12 matrix Σ is decomposed as follows:

$$\hat{\Sigma} = \begin{pmatrix} \cdots & \cdots \\ \cdots & \hat{K} \end{pmatrix}, \quad \hat{\Sigma}^{-1} = \begin{pmatrix} \hat{\Xi}^{-1} & \cdots \\ \cdots & \cdots \end{pmatrix}, \quad (26)$$

where the 8×8 block $\hat{K}$ "works" in the space of all derivatives of RGFs. It was shown that $\det \hat{\Sigma} = \det \hat{K} \det \hat{\Xi}$ [29]. The next trick is to introduce differential operators to present the charge correlation function as [29]

$$\frac{1}{(2\pi)^2\rho^2\sqrt{\det \hat{K}}}\int d^8\mathbf{t}\ \exp\left(-\frac{1}{2}\mathbf{t}\hat{\Xi}\mathbf{t}\right)J_{\nabla}J_{\nabla S}\delta^8(\mathbf{t}). \quad (27)$$

Then we obtain

$$G_q(s) = \frac{1}{(2\pi)^2\rho^2}\frac{1}{\sqrt{\det \hat{K}}}W, \quad (28)$$

where

$$W = [J_{\nabla}J_{\nabla s}\exp(-\mathbf{t}\hat{\Xi}\mathbf{t}/2)]|_{t=0}. \quad (29)$$

Dennis also presented a procedure to calculate the matrix elements of the block $\hat{\Xi}$. Continuing this tedious procedure, we finally obtain

$$W = 2L^2 + IF + HG - \frac{8ECD^2}{(1-4B^2)(1-4A^2)} + \frac{4E^2D^2(1+8B^2)}{(1-4B^2)^2} + \frac{4C^2D^2(1+8A^2)}{(1-4A^2)^2} - \frac{4B(GE^2+2LED+HD^2)}{1-4B^2} - \frac{4A(IC^2+2LCD+FD^2)}{1-4A^2} \quad (30)$$

and

$$\det \hat{\Xi} = \left(\frac{1}{4}-A^2\right)\left(\frac{1}{4}-B^2\right). \quad (31)$$

A plot of $G_q(s)$ based on formulas (25), (28), (30), and (31) is given in Fig. 6. Note that in Fig. 6 and what follows we rescaled the distance $s \to \sqrt{\rho}s$.

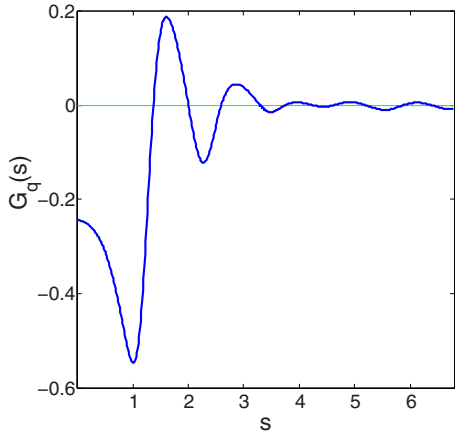

FIG. 6. (Color online) The charge density correlation function (22) for the random elastic in-plane waves (6). $\sigma=0.345$.

Using formula (12) we present the density correlation function of NPs, Eq. (21), as follows:

$$G(s) = \frac{1}{\pi^2}\int\int \frac{d\omega_1 d\omega_2}{\omega_1\omega_2}\frac{\partial^2\langle\delta(u)\delta(v)\delta(u_s)\delta(v_s)e^{i\omega_1 J + i\omega_2 J_s}\rangle}{\partial\omega_1\,\partial\,\omega_2}, \tag{32}$$

with an average over RGFs of

$$\begin{aligned}\langle\cdots\rangle &= \frac{1}{(2\pi)^6\sqrt{\det\hat{\Sigma}}}\int d^{12}\varphi\ \delta(u)\delta(v)\delta(u_s)\delta(v_s)\\ &\times\exp(i\omega_1 J + i\omega_2 J_s - \varphi\hat{\Sigma}^{-1}\varphi^T/2)\\ &= \frac{1}{(2\pi)^6\sqrt{\det\hat{\Sigma}}}\int \exp(i\mathbf{y}\hat{\Omega}\mathbf{y}^T - \mathbf{y}\hat{\Sigma}_1^{-1}\mathbf{y}^T/2)d^8\mathbf{y}.\end{aligned} \tag{33}$$

Here $\mathbf{y}=[u_x,u_y,v_x,v_y,u_x^s,u_y^s,v_x^s,v_y^s]$ and $\hat{\Sigma}_1=\langle\mathbf{y}^T\mathbf{y}\rangle$ is a block of $\hat{\Sigma}^{-1}$. Moreover,

$$\hat{\Omega} = \frac{1}{2}\begin{pmatrix} & & & \omega_1 & & & & \\ & & -\omega_1 & & & & & \\ & -\omega_1 & & & & & & \\ \omega_1 & & & & & & & \\ & & & & & & & \omega_2 \\ & & & & & & -\omega_2 & \\ & & & & & -\omega_2 & & \\ & & & & \omega_2 & & & \end{pmatrix}. \tag{34}$$

The average (33) results in

$$\langle\cdots\rangle = \frac{1}{(2\pi)^2\sqrt{\det(\hat{\Sigma})}}\frac{1}{\sqrt{\det[-i\hat{\Omega}(\omega_1,\omega_2)+\hat{\Sigma}_1^{-1}]}}.$$

However, the calculation of these determinants is a very tedious procedure. Moreover, the next step of the calculation of integrals over ω_1 and ω_2 can be performed only numerically. Therefore, at each point ω_1,ω_2 we calculated the determinant numerically with further summation over these frequencies. The final result for the density correlation function is shown in Fig. 7.

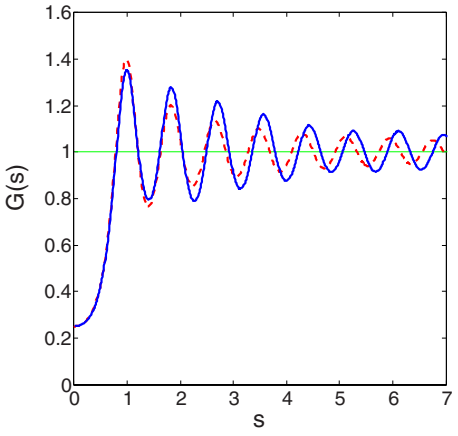

FIG. 7. (Color online) The density correlation function (21) for in-plane random elastic waves (6) for $\sigma=0.345$ (solid line) compared to that of the quantum chaotic wave function (dashed line) given in [25,26].

IV. DISTRIBUTION OF NEAREST DISTANCES BETWEEN NPs

Knowledge of the density correlation function (21) allows us to calculate the distribution function of the nearest distances between NPs. Following [26] we use here two approximations. According to Poisson's law the probability that no other points belong to a circle with dimensionless radius s centered at any given one is given by

$$P(0,s) = \exp[-\langle n(s)\rangle]. \tag{35}$$

Taking into account that the mean number of NPs inside the circle of radius s around a given one is

$$\langle n(s)\rangle = 2\pi\rho\int_0^s rG(r)dr, \tag{36}$$

we can write the Poisson approximation of the distribution of nearest distances between NPs in the form

$$f(s) = 2\pi\rho s G(s)\exp[-\langle n(s)\rangle]. \tag{37}$$

The Bernoulli approximation is introduced in [26] to describe the competition among NPs to be the nearest neighbor of the given one. It suggests that uncorrelated competing NPs occur outside the circle with probability

$$P(0,s) = \left(1 - \frac{\langle n(s)\rangle}{n}\right)^n, \tag{38}$$

where n is the number of competing points; hence,

$$f(s) = 2\pi\rho s G(s)[1 - \langle n(s)\rangle/3]^2, \tag{39}$$

in case only three NPs are competing. Both distributions are shown in Figs. 8 and 9 compared to numerical results. For

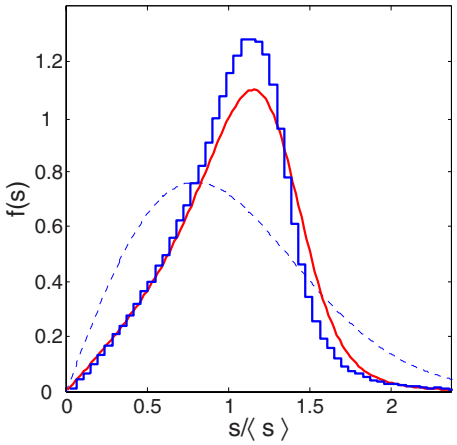

FIG. 8. (Color online) Histogram of the distribution function of the nearest distances between NPs for the random in-plane random elastic waves (6). $\sigma=0.345$. The solid line shows the distribution function calculated in the Poisson approximation (37). The dashed line shows the special case of uniformly distributed and completely random points [37] $f(x)=\frac{\pi x}{2}\exp(-\pi x^2/4)$.

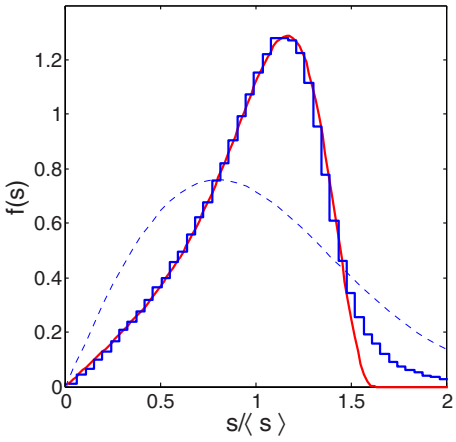

FIG. 9. (Color online) The same as in the previous figure except that the distribution function of the nearest distances between NPs is given in the Bernoulli approximation (39).

numerical statistics we accumulated the nearest distances between more than 500 000 NPs for 120 realizations of the random superpositions of 100 plane waves (6). The resulting histogram is shown in Figs. 8 and 9. One can see that the Bernoulli approximation fits the numerical histogram in the vicinity of the mean distance between NPs better as compared to the Poisson approximation. The reason is that the Bernoulli approximation takes into account the competition between neighboring points to be the nearest one of the given NP. However, with an increase of the distance s the Bernoulli approximation becomes invalid for any n because $\langle n(s)\rangle$ exceeds n.

V. CONCLUSION

While the flexural eigenmodes of elastic billiards are featured by nodal lines, the in-plane eigenvibrations are characterized by nodal points. By that, in-plane vibrations are similar to the complex quantum wave function which describes open two-dimensional quantum billiards [25–27,35,36]. However, the nodal points of in-plane vibrations have more rich variety. They might be nodes, centers, focuses, and saddles (Figs. 1–3) as dependent on the superposition of longitudinal and transverse in-plane waves. In turn, that dependence is defined by the material parameter σ which affects the mean density of NP as shown in Fig. 4, the density correlation function, and correspondingly the distribution function of the nearest distances between NPs. However, surprisingly, after rescaling of the distance $s\to s\sqrt{\rho}$ that effect is not profound as was expected. As shown in Fig. 7 the density correlation functions for the in-plane random waves and for the complex random waves [25,26] are close to each other. Correspondingly the distribution functions of the nearest distances for both cases turned out to be very close to each other too. For this reason the comparison is not shown here. The reason lies in a geometric origin of NPs as a result of the intersection of the nodal lines of $u=0$ and $v=0$ for the elastic case or the nodal lines of the real and imaginary parts of the complex wave function for the quantum case [34,35]. Although local patterns of nodal lines are different, they become equivalent after statistical averaging. As a result, the density correlation function very weakly depends on the material parameter σ. Therefore we can conclude that the distribution function of the nearest distances between NPs can serve as a signature of wave chaos not only for chaotic quantum billiards [35], but also for elastic billiards.

ACKNOWLEDGMENTS

Authors are grateful to K.-F. Berggren and E. N. Bulgakov for stimulating discussions. This work has been supported by the Royal Swedish Academy of Sciences for collaboration between Sweden and Russia and RFBR Grant No. 07-02-00694.

APPENDIX

The matrix elements of correlation matrix (24) are

$$A=\gamma a(k_l s)+(1-\gamma)b(k_t s),$$

$$B=\gamma a(k_l s)+(1-\gamma)b(k_t s),$$

$$C=\gamma\frac{da(k_l s)}{ds}+(1-\gamma)\frac{db(k_t s)}{ds},$$

$$D=\gamma\frac{db(k_l s)}{ds}-(1-\gamma)\frac{db(k_t s)}{ds},$$

$$E=\gamma\frac{db(k_l s)}{ds}+(1-\gamma)\frac{da(k_t s)}{ds},$$

$$F=-\gamma\frac{d^2a(k_l s)}{ds^2}-(1-\gamma)\frac{d^2b(k_t s)}{ds^2},$$

$$G = -\gamma\frac{d^2b(k_ls)}{ds^2} + (1-\gamma)\left(k_t^2 b(k_ts) + \frac{d^2b(k_ts)}{ds^2}\right),$$

$$H = -\gamma\frac{d^2b(k_ls)}{ds^2} - (1-\gamma)\frac{d^2a(k_ts)}{ds^2},$$

$$I = \gamma\left(k_l^2 b(k_ls) + \frac{d^2b(k_ls)}{ds^2}\right) - (1-\gamma)\frac{d^2b(k_ts)}{ds^2},$$

$$L = -\gamma\frac{d^2b(k_ls)}{ds^2} + (1-\gamma)\frac{d^2b(k_ts)}{ds^2}, \tag{A1}$$

where

$$a(x) = -J_0''(x) = \frac{1}{2}[J_0(x) - J_2(x)],$$

$$b(x) = J_0(x) - J_0''(x) = \frac{1}{2}[J_0(x) + J_2(x)],$$

$$f = F(0) = I(0) = \frac{3\gamma k_l^2}{8} + \frac{(1-\gamma)k_t^2}{8},$$

$$g = G(0) = H(0) = \frac{\gamma k_l^2}{8} + \frac{3(1-\gamma)k_t^2}{8},$$

$$l = L(0) = \frac{\gamma k_l^2}{8} - \frac{(1-\gamma)k_t^2}{8}. \tag{A2}$$

[1] R. L. Weaver, J. Acoust. Soc. Am. **85**, 1005 (1989).
[2] C. Ellegaard, T. Guhr, K. Lindemann, J. Nygård, and M. Oxborrow, Phys. Rev. Lett. **77**, 4918 (1996).
[3] O. Legrand, C. Schmitt, and D. Sornette, Europhys. Lett. **18**, 101 (1992).
[4] K. Schaadt and A. Kudrolli, Phys. Rev. E **60**, R3479 (1999).
[5] P. Bertelsen, C. Ellegaard, and E. Hugues, Eur. Phys. J. B **15**, 87 (2000).
[6] A. Andersen, C. Ellegaard, A. D. Jackson, and K. Schaadt, Phys. Rev. E **63**, 066204 (2001).
[7] K. Schaadt, T. Guhr, C. Ellegaard, and M. Oxborrow, Phys. Rev. E **68**, 036205 (2003).
[8] K. F. Graff, *Wave Motion in Elastic Solids* (Dover, New York, 1975).
[9] L. D. Landau and E. M. Lifshitz, *Theory of Elasticity* (Pergamon, Oxford, 1959).
[10] M. D. Waller, Proc. R. Soc. London, Ser. A **211**, 265 (1952).
[11] B. Thomas and A. M. Squires, Phys. Rev. Lett. **81**, 574 (1998).
[12] I. S. Aranson and L. S. Tsimring, Rev. Mod. Phys. **78**, 641 (2006).
[13] M. Dorrestijn, A. Bietsch, T. Acikalin, A. Raman, M. Hegner, E. Meyer, and C. Gerber, Phys. Rev. Lett. **98**, 026102 (2007).
[14] J. D. Achenbach, *Wave Propagation in Elastic Solids* (North-Holland, Amsterdam, 1973).
[15] D. N. Maksimov and A. F. Sadreev, Pis'ma Zh. Eksp. Teor. Fiz. **86**, 664 (2007) [JETP Lett. **86**, 670 (2007)].
[16] Lord Rayleigh, *The Theory of Sound* (Dover, New York, 1945).
[17] A. I. Shnirelman, Usp. Mat. Nauk **29**, 181 (1974).
[18] A. Voros, Ann. Inst. Henri Poincare, Sect. A **24**, 31 (1976).
[19] M. V. Berry, J. Phys. A **10**, 2083 (1977).
[20] K. J. Ebeling, Opt. Acta **26**, 1505 (1979); *Statistical Properties of Random Wave Fields in Physical Acoustics: Principles and Methods* (Academic Press, New York, 1984).
[21] R. Pnini and B. Shapiro, Phys. Rev. E **54**, R1032 (1996).
[22] H.-J. Stöckmann, *Quantum Chaos: An Introduction* (Cambridge University Press, Cambridge, England, 1999).
[23] B. I. Halperin, in *Statistical Mechanics of Topological Defects*, edited by R. Balian, N. Kleman, and J.-P. Poirer (North Holland, Amsterdam, 1981).
[24] F. Liu and G. F. Mazenko, Phys. Rev. B **46**, 5963 (1992).
[25] M. V. Berry and M. R. Dennis, Proc. R. Soc. London, Ser. A **456**, 2059 (2000); **457**, 2251 (2001).
[26] A. I. Saichev, K.-F. Berggren, and A. F. Sadreev, Phys. Rev. E **64**, 036222 (2001).
[27] M. Barth and H.-J. Stöckmann, Phys. Rev. E **65**, 066208 (2002).
[28] G. Foltin, J. Phys. A **36**, 1729 (2003).
[29] M. R. Dennis, J. Phys. A **36**, 6611 (2003).
[30] Y.-H. Kim, M. Barth, U. Kuhl, and H.-J. Stöckmann, Prog. Theor. Phys. **150**, (Suppl.), 105 (2003).
[31] B. A. Dubrovin, A. T. Fomenko, and S. P. Novikov, *Modern Geometry: Methods and Applications*, Graduate Texts in Mathematics, Vol. 104 (Springer-Verlag, New York, 1985), Pt. II.
[32] B. I. Halperin, in *Physics of Defects*, edited by R. Balian *et al.* (North-Holland, Amsterdam, 1981).
[33] N. D. Mermin, Rev. Mod. Phys. **51**, 591 (1979).
[34] N. Shvartsman and I. Freund, Phys. Rev. Lett. **72**, 1008 (1994).
[35] K.-F. Berggren, A. F. Sadreev, and A. A. Starikov, Phys. Rev. E **66**, 016218 (2002).
[36] A. I. Saichev, H. Ishio, A. F. Sadreev, and K.-F. Berggren, J. Phys. A **35**, L87 (2002).
[37] J. R. Eggert, Phys. Rev. B **29**, 6664 (1984).